

Article

Simulation Tool for the Development of a Staged Combustion Pellet Stove Controller

Daniel Lustenberger , Joris Strassburg, Tom Strebel, Fabienne Mangold  and Timothy Griffin *

Institute of Biomass and Resource Efficiency, University of Applied Sciences Northwestern,
5210 Windisch, Switzerland

* Correspondence: timothy.griffin@fhnw.ch

Abstract: Optimizing the combustion control concepts on a pellet stove with very low heat output is time-consuming and costly. In order to shorten the required laboratory test time, a 0-D transient tool was developed within the ERA-NET project “LowEmi-MicroStove”, which simulates a 4 kW pellet stove with staged combustion and heat transfer. This approach was chosen in order to greatly simplify the description of the combustion processes and so reduce the computational complexity and simulation time. The combustion of a bed of pellets is modeled as a superposition of the combustion cycles of individual pellets, assuming no interactions between pellets. A test setup was developed and used to determine the ignition and burning cycle of individual pellets. The description of the CO emissions behavior is based upon an empirically grounded relation which is in turn based on the air/fuel ratio and the combustion chamber temperature. For the validation of the 0-D simulation results, a test rig for a 4 kW pellet stove was built. Despite its simplistic approach, good agreement was found between the simulation and 4 kW pellet stove test results for the mean values and temporal fluctuations of flue gas temperature and oxygen and carbon monoxide content during start up, stable operation and load changes. The simulation could thus be used to quantify the effect of air flow rates and distribution as well as load changes on performance and draw conclusions regarding different process control strategies. A control strategy which can operate the stove at high temperatures near the air stoichiometric limit with acceptable CO emissions has been proven to be the most promising. Additionally, the model can be used to quantify the effects of variations in other process parameters, for example the impact of fluctuations in the pellet feed. Due to its effectiveness and simplicity, this model approach can be applied for the development of control strategies for other staged, pellet combustion systems.

Keywords: wood combustion; transient combustion model; pellet stove simulation; staged combustion; combustion air control strategy



Citation: Lustenberger, D.; Strassburg, J.; Strebel, T.; Mangold, F.; Griffin, T. Simulation Tool for the Development of a Staged Combustion Pellet Stove Controller. *Energies* **2022**, *15*, 6969. <https://doi.org/10.3390/en15196969>

Academic Editors: Yaojie Tu and Qingguo Peng

Received: 22 August 2022

Accepted: 15 September 2022

Published: 23 September 2022

Publisher’s Note: MDPI stays neutral with regard to jurisdictional claims in published maps and institutional affiliations.



Copyright: © 2022 by the authors. Licensee MDPI, Basel, Switzerland. This article is an open access article distributed under the terms and conditions of the Creative Commons Attribution (CC BY) license (<https://creativecommons.org/licenses/by/4.0/>).

1. Introduction

Wood pellets are, next to wood logs, the leading biomass fuel for heating systems in residential buildings throughout Europe [1]. In recent years, the energy efficiency of buildings has been gradually improved, so that a trend toward heating systems with low output (<10 kW) can be observed on the market. Pellet boilers can no longer fully satisfy this market demand due to their larger nominal heat output. Therefore, pellet stoves, which are usually designed as space heaters for a lower nominal output range of about 6 to 10 kW, have gained interest. Currently, there is increasing interest in heating systems with even lower nominal outputs which are suitable for low-energy or passive houses [2–4]. In an Eranet project, an international team designed a pellet stove with a nominal output of 4 kW [5].

Reducing the nominal output of stoves reduces their volume. This leads to a less favorable surface-to-volume ratio as compared to stoves with higher output, which results

in higher heat radiation and thus lower temperatures in the combustion chamber. Fluctuations in the fuel supply and false air contributions also play an important role. These factors make low-pollution operation of a low-power heating system difficult across all operating phases. These problems can be reduced by regulating the combustion air supply [6]. The state of the art for pellet stoves in the field is to control the air supply through a fixed setpoint for the combustion chamber outlet temperature without taking the combustion quality (e.g., CO emissions) into account.

To compete with other heating systems such as heat pumps, it is important that pellet stoves with low heat output have low production costs. For this reason, the combustion air control system should use as few sensors as possible, and its regulation should not require too much computational complexity so that it can be implemented on a conventional stove control system. For this purpose, different strategies must be developed and compared with each other in terms of their operational behavior and complexity. Then the most suitable strategies must be tested for their stability. These stability tests can be very time-consuming, since certain operating states of the stove only occur after several hours of operation due to the transient heating up of the system.

Currently, there is no tool available that sufficiently simulates the transient behavior of a pellet stove and system dependency on important process control parameters (actuators), such as the air flows, which can also be used to efficiently test the suitability of different control strategies. Thus, the optimization of control strategies requires costly test campaigns which are a barrier to process improvement.

Gölles (2009) [7] used a model to simulate a wood-fired heating boiler. This model was developed as a model-based control, but not to test control strategies external to the model. The tool developed for this project allows one to test the suitability of control strategies for pellet stoves by connecting a controller programmed in LabView to the model. Our tool reacts to controller-triggered parameter changes in the same way as the real pellet stove, allowing for optimization of the control strategy. In addition, critical operating states of the stove can be deliberately induced in the simulation in order to test the stability of the control system. The aim of the tool is therefore not to represent the detailed combustion processes exactly, but to simulate the impact of process variables relevant for control. These are the temperature at the combustion chamber outlet and the oxygen content and CO emissions in the flue gas. For this reason, the details of the combustion process are represented in a very simplified way.

2. Simulation Tool

The simulation tool programmed in a MATLAB–Simulink R2021b environment consists of five individual modules that can together simulate a generic pellet stove with staged combustion. The modular setup allows one to increase the complexity of each module step by step and to simplify the traceability of changes. A schematic of a typical stove, with the individual components, is shown in Figure 1. The reactor consists of a primary (1) and a secondary (2) combustion zone. The air mass flow required for gasification and combustion is controlled by a fan (3) and divided between primary (4) and secondary (5) air via a flap. Via a screw (6) driven by a motor (M), pellets are fed to the primary zone where they are heated up and ignited. Product gas from the primary zone rises into the secondary zone, where it is then oxidized, reaches its flame temperature and transfers heat to the combustion chamber wall (7). Due to this heat loss, the exhaust gas cools down on its way from the burnout zone to the outlet, which has an important influence on the CO emissions. Depending on the control concept, various parameters are measured in different combinations at the outlet, such as the temperature, the O₂ or the CO content. Based on these values, the process control (8) should adjust the actuators (pellet supply, fan speed, flap position) so that emissions are minimized.

The described model above is shown as a diagram in a MATLAB–Simulink environment in Figure 2. Each of the five modules is represented by a block. A simulation step is performed for each time step of one second in real time, and the calculated results are used

in the next simulation step as inputs for another block. Arrows indicate the dependencies. The individual modules are described in more detail in Sections 2.1–2.4.

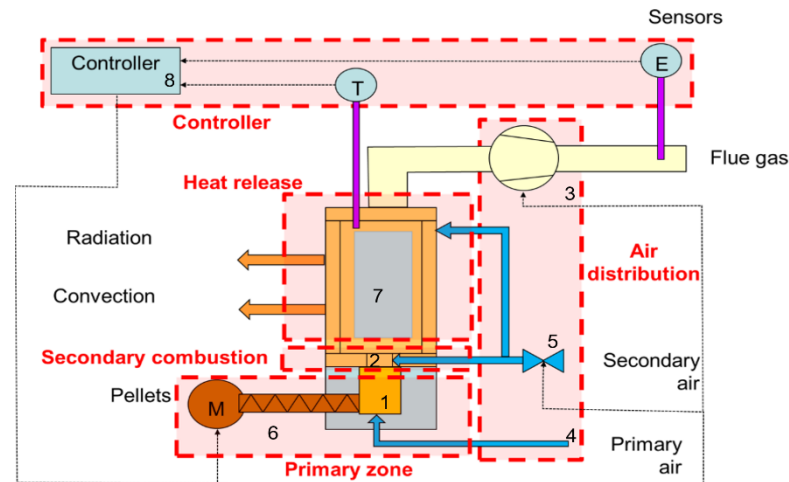


Figure 1. Typical construction of a two-stage combustion stove.

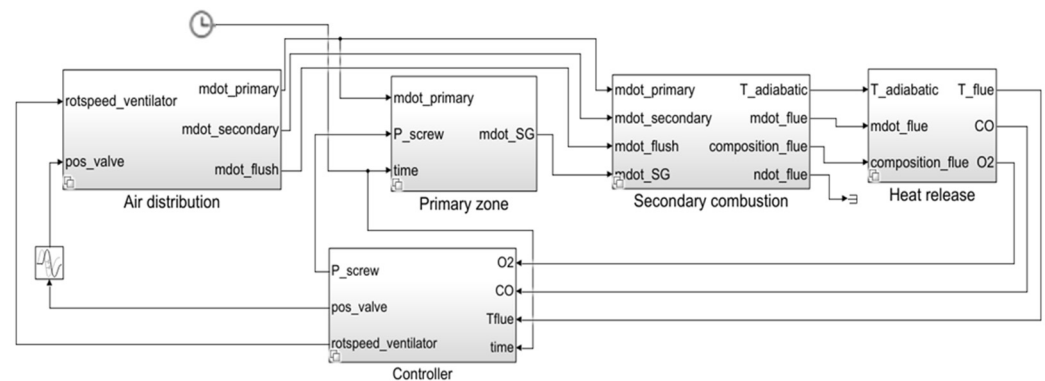


Figure 2. MATLAB–Simulink model of the digital twin.

2.1. Air Distribution

Based on the fan speed and the secondary air flap position specified by the controller module, the primary and secondary air mass flow rates are calculated in this module. A possible approach to simulate the air distribution module in a staged combustion process is described in [8]. The schematics of an adapted version of this module are shown in Figure 3. The individual resistances that form the basis for the calculation of the primary air and secondary air supply in this module are derived below.

There are three constant pipe resistances: $R_{P,P}$, $R_{P,S}$ and R_{HX} . The variable resistance $R_{F,S}$ reflects different secondary air flap positions. The resistances are determined via the general formula for a pressure drop Δp , where R is the resistance and \dot{V} the volume flow rate.

$$\Delta p = R \dot{V}^2 \quad (1)$$

With measurements of the primary air volume flow rate \dot{V}_P , ambient pressure p_{amb} and combustion chamber pressure p_{CC} , the primary air resistance $R_{P,P}$ can be determined.

$$R_{P,P} = \frac{p_{amb} - p_{CC}}{\dot{V}_P^2} \quad (2)$$

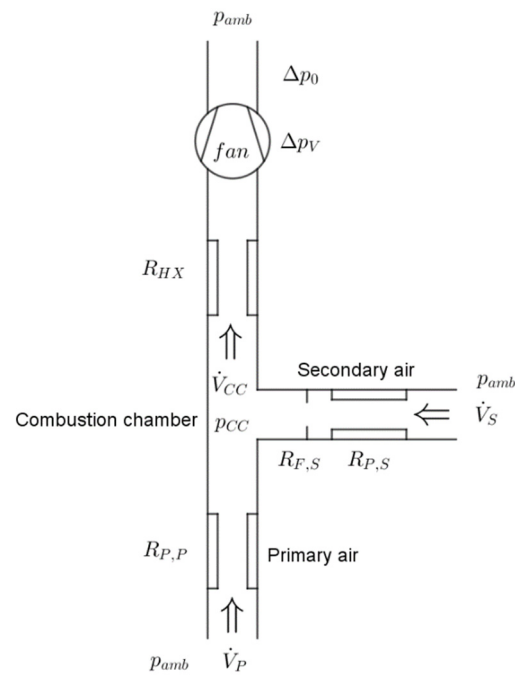


Figure 3. Scheme of air mass flow with fan and division into primary air and secondary air.

The resistance $R_{F,S}$ in the secondary air supply (see Figure 3) can be neglected when the secondary air flap position (SAFP) is 100% opened. Under these conditions the pipe resistance of the secondary air supply $R_{P,S}$ can be determined similarly to the pipe resistance of the primary air supply. \dot{V}_S represents the measured secondary air volume flow rate.

$$R_{P,S} = \frac{p_{amb} - p_{CC}(\text{SAFP} = 100\%)}{\dot{V}_S^2} \quad (3)$$

The total resistance in the secondary air supply is the sum of $R_{P,S}$ and $R_{F,S}$. The secondary air flap resistance $R_{F,S}$ for different SAFP can be calculated by applying Equation (1) to the secondary air supply.

$$R_{F,S}(\text{SAFP}) = \frac{p_{amb} - p_{CC}(\text{SAFP})}{\dot{V}_S(\text{SAFP})^2} - R_{P,S} \quad (4)$$

The resistance at the heat exchanger (downstream of the secondary air inlet until the fan inlet) is calculated as follows,

$$R_{HX} = \frac{p_{CC} - (p_{amb} - \Delta p_V - \Delta p_0)}{(\dot{V}_S + \dot{V}_P)^2} = \frac{p_{CC} - (p_{amb} - \Delta p_V - \Delta p_0)}{\dot{V}_{tot}^2} \quad (5)$$

where Δp_V is determined by the fan characteristic, and Δp_0 is the chimney draft. Finally, all resistances are determined and can be implemented in the air distribution module.

In the module, the volume flow rates \dot{V}_P and \dot{V}_S are calculated by solving Equations (2) to (5). The non-linear system of equations with its four unknown variables \dot{V}_P , \dot{V}_S , Δp_V and p_{CC} can be solved via an iterative method by considering the fan characteristics. The fan characteristics describes the dependence of the conveyed volume flow rate by the fan and the pressure drop Δp_V .

2.2. The Primary Combustion Chamber

This module aims to describe the pellet gasification process by using the pellet intake expressed by a probability function and the primary airflow calculated in the air distribution module.

There are modeling approaches to describe the pellet gasification process in a stove [9], but these are complex and difficult to implement in a transient model as required here [10]. A different approach was taken, assuming that heat release during normal operation can be directly linked to the individual pellet mass loss cycle, which can be measured and mathematically described. Although some measurements on pellet mass loss are available [11,12], no data for staged combustion were found. Therefore, a new test rig has been constructed for measuring the pellet mass loss. Typical conditions for two-stage combustion (temperature and air flow rates) were maintained while a single pellet is fed onto the pellet grate. Preheated primary air is supplied from below and secondary air from above (see Figure 4a).

To determine the total instantaneous pellet gas mass flow, the respective mass flows of the life cycle stages of the individual pellets are summed up, which can be seen in Equation (6) and Figure 4b. The primary energy consumption rate, or heat input in the model is assumed to be proportional to the mass loss, using the net calorific value.

$$m(t) = \sum_i m_i(t) \quad (6)$$

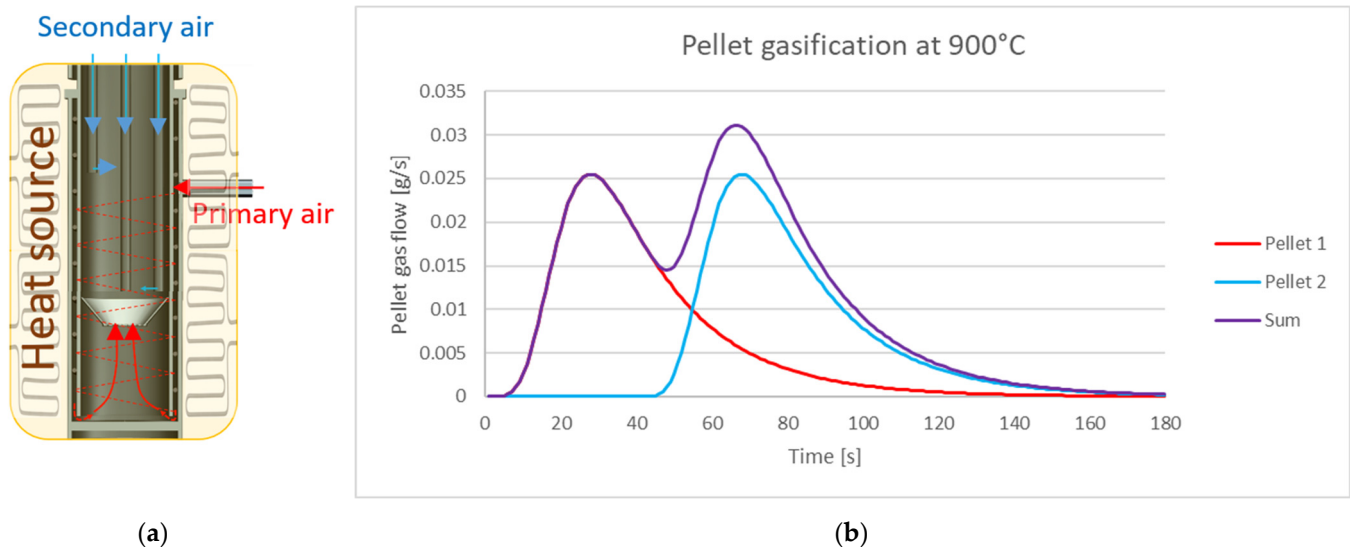


Figure 4. Test rig to measure pellet mass loss (a) and the corresponding pellet gas flow (b).

In the next step, a fit function is sought for the pellet mass loss, i.e., the gasification of a single pellet as a function of time for the different temperatures. In civil engineering, moisture transport in wood drying is described by a vapor pressure gradient of water [13]. This approach is applied also to the gasification products in the wood. Due to the transient heating of the pellet to the pellet grate temperature, the pellet is dried, and pyrolysis and gasification processes cause gases (e.g., hydrocarbons) to be formed and transported from the inside of the pellet to the surroundings. Concentration gradients cause the gases to start flowing out of the pellet. The assumption here is that the formation of gases (their partial pressure in the pellets) is highly temperature dependent (like the vapor pressure of water in wet wood) and that heat and mass transfer of the pellet gases and water vapor in moisture transport can be described similarly.

To simulate the transient heating of the pellet, a fitted error function was used (7). We use this to calculate an average temperature of the pellet T_x as a function of time. T_g is the

constant ember bed temperature, and T_0 is the temperature of the pellet at the beginning of the process (time $t = 0$). To adjust the heating rate, μ serves as a fit parameter.

$$\operatorname{erf}(\mu t) = \theta = \frac{T_x - T_g}{T_0 - T_g} \quad (7)$$

The transport of the gasification products from the pellet is controlled by the diffusion density g in the radial direction x , see (8). The driving force here is a partial pressure difference from the pellet, p_{dx} , to the environment, in which the gasification products have been oxidized. D_v is the gas diffusion coefficient and Δp_v the vapor pressure difference.

$$g = -D_v * \Delta p_v * x = -D_v * (p_{dx} - 0) * x \quad (8)$$

The partial pressure of the gasification products p_{dx} is calculated with Equation (9) [14] and depends on the current pellet temperature T_x and the mean “boiling point” of all substances in the pellet T_s (estimated by thermogravimetric analysis). The substance constant a serves as a fit parameter.

$$p_{dx} = p_0 * e^{(1 - \frac{T_s}{T_x}) * a} \quad (9)$$

The diffusion flow density g is multiplied by the surface area A of the pellet and the time step t , to obtain the mass loss Δm . The mass loss is also dependent on the mass of the pellet that has not yet been gasified m_{rest} in relation to the mass at the beginning of the combustion m_{tot} . In summary, the mass loss of a pellet is given by (10).

$$\Delta m(t) = -\frac{m_{rest}}{m_{tot}} * A * t * g \quad (10)$$

In Figure 5 the result of the fit formula is compared with that of the experimental setup. Here, one gram of pellet was burnt at a temperature of 800 °C.

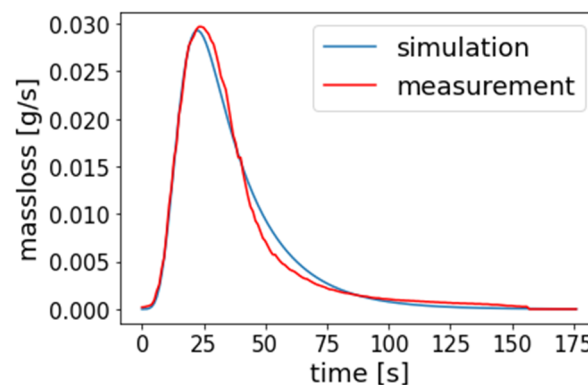


Figure 5. Comparison of the measured and simulated mass loss of three pellets with a total weight of 1 g, temperature combustion chamber 800 °C, primary air flow 0.2 g/s and secondary air flow 0.15 g/s.

The simulated peak has a maximal deviation of 0.001 g/s compared to the measurement.

2.3. Secondary Combustion

From the air distribution module, the amount of combustion air is transferred to the secondary combustion module. The products of wood pellet gasification with the primary air in the primary zone flow into the secondary combustion zone where they are fully oxidized. An equilibrium calculation was used to determine the composition of the gasification products resulting from the mass loss of wood, using a substitute fuel for the wood [15]. The substitute fuel (consisting of H_2 , H_2O , CO_2 , CO and C_3H_8) has the same

thermodynamic properties and the same elemental composition as wood pellets. Thus, the elemental composition of the exhaust gas matches the exhaust gas composition when burning wood pellets and the absolute enthalpy (or calorific value) of the substitute fuel is identical to that of wood pellets. Subsequently, the flue gas composition and the adiabatic flame temperature can be calculated iteratively via the mass flows (substitute fuel, primary and secondary air). The adiabatic flame temperature is needed in the following heat release module to estimate the heat loss.

2.4. Heat Release Module

In the heat release module, the heat transfer and cooling of the combustion products is calculated and the emissions in the flue gas are determined.

Figure 6 shows the energy balance of the combustion chamber. It is assumed that hot combustion products with adiabatic flame temperature T_{ad} calculated in the secondary combustion module enters the combustion chamber. Heat exchange to the insulation $\dot{Q}_{ins,i}$ and heat release to the surroundings through a window \dot{Q}_{win} , cool down the product gas to the flue gas temperature T_{flue} . The energy balance of the stove is represented by the following equation.

$$\dot{m}_{flue} c_{p,flue} (T_{ad} - T_{flue}) = \dot{Q}_{win} + \dot{Q}_{ins,i} \quad (11)$$

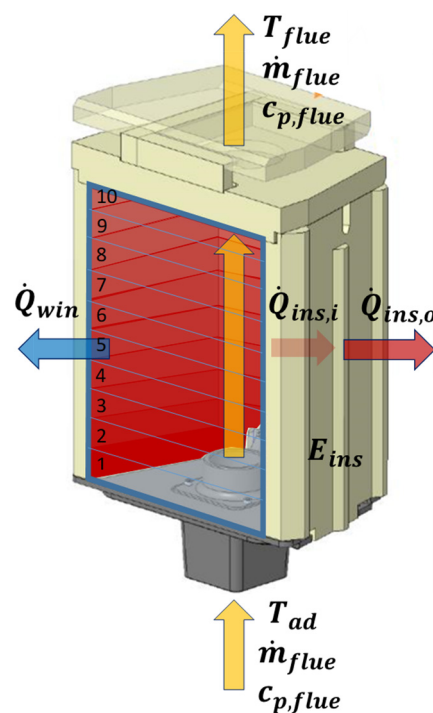


Figure 6. Energy and mass balance of the combustion chamber.

The model represents the transient behavior of the stove through the heat storage in the insulation

$$\frac{dE_{ins}}{dt} = \dot{Q}_{ins,i} - \dot{Q}_{ins,o} \quad (12)$$

To simplify the calculation, thermal resistances for a cylindrical combustion chamber are introduced, using estimated values for the combustion chamber as well as values obtained from our partners for the specific stove investigated in this project (see Figure 7), which can be summarized with three resistances R_{win} , $R_{ins,i}$, $R_{ins,o}$. At a combustion chamber outlet temperature of 700 °C (see Equations (13)–(15)), the thermal resistance over the whole window $R_{win} = 0.36$ K/W is much smaller than the total resistance over the insulation $R_{ins,i} + R_{ins,o} = 2.24$ K/W. Therefore, the heat loss occurs mainly over the window. The resistance of the window can be divided into a radiation

resistance $R_{win,rad} = 0.44$ K/W and a resistance containing convection and conduction $R_{win,conv,i} + R_{win,cond} + R_{win,conv,o} = 2.31$ K/W. Comparing these two resistances for the specific MPS stove, radiation over the window can be identified as the main source for the heat loss from the exhaust gas in the combustion chamber.

$$R_{win} = \frac{(R_{win,conv,i} + R_{win,cond} + R_{win,conv,o})R_{win,rad}}{R_{win,conv,i} + R_{win,cond} + R_{win,conv,o} + R_{win,rad}} = 0.36 \text{ K/W} \quad (13)$$

$$R_{ins,i} = R_{ins,cond,1} + \frac{R_{ins,rad}R_{ins,conv}}{R_{ins,rad} + R_{ins,conv}} = 1.51 \text{ K/W} \quad (14)$$

$$R_{ins,o} = R_{ins,cond,2} + R_{w,cond} + \frac{R_{w,rad}R_{w,conv}}{R_{w,rad} + R_{w,conv}} = 0.73 \text{ K/W} \quad (15)$$

In order to improve the accuracy of the calculated flue gas temperature in the model, the combustion chamber was divided into 10 sections as shown in Figure 6. The calculation routine for the flue gas temperature is shown in Figure 8. The procedure is as follows:

1. In the first step, all heat flows $\dot{Q}_{win}(j, t)$, $\dot{Q}_{ins,i}(j, t)$ and $\dot{Q}_{ins,o}(j, t)$ for one section (j) are determined with knowledge of the flue gas $T_{flue}(j, t)$ and insulation temperatures $T_{ins}(j, t)$. For the first section ($j = 1$), it is assumed that the flue gas temperature $T_{flue}(1, t)$ corresponds to the adiabatic flame temperature. For the first timestep ($t = 1$), the temperature of the insulation $T_{ins}(j, 1)$ is equal to the ambient temperature.
2. In the second step, the heat flows calculated in step 1 are used as inputs to calculate the exit temperature $T_{flue}(j + 1, t)$ for the next section ($j + 1$). The routine continues with step 1 for the new section. The calculations are repeated until the outlet temperature of the last, 10th, section is determined. In this case, step 3 is carried out.
3. In the third step, new insulation temperatures ($T_{ins}(j, t + 1)$) are calculated for a new timestep ($t + 1$). Afterwards the calculation routine continues with step 1 in the first section ($j = 1$).

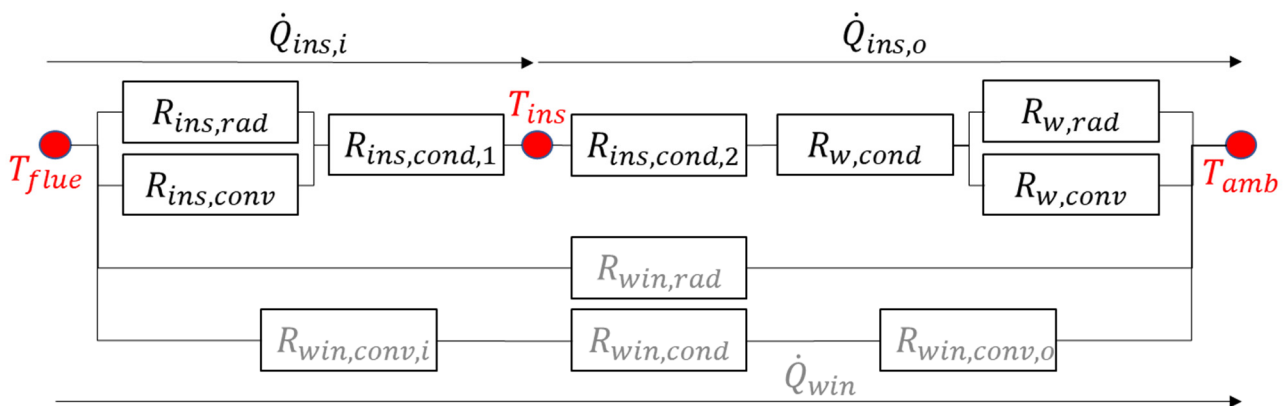


Figure 7. Thermal resistance diagram of the stove wall and window.

In the simulation tool, the CO emissions are simulated using empirical values from a real pellet stove. Since the decomposition of hydrocarbons is much faster than the further oxidation of CO to CO₂, the emissions of unburned hydrocarbons are not considered [16]. The NO_x emissions are also not simulated.

The CO concentration in the flue gas is a function of the residual oxygen content in the flue gas and the dependence in a CO-O₂ plot has the form of an upward-opening parabola (see Figure 9). The parabola shifts with the increase in operating time caused by higher combustion chamber temperatures towards lower CO emissions, at a lower oxygen content [17]. This makes it necessary to continually adjust this functionality during the operation and during the simulation of the combustor.

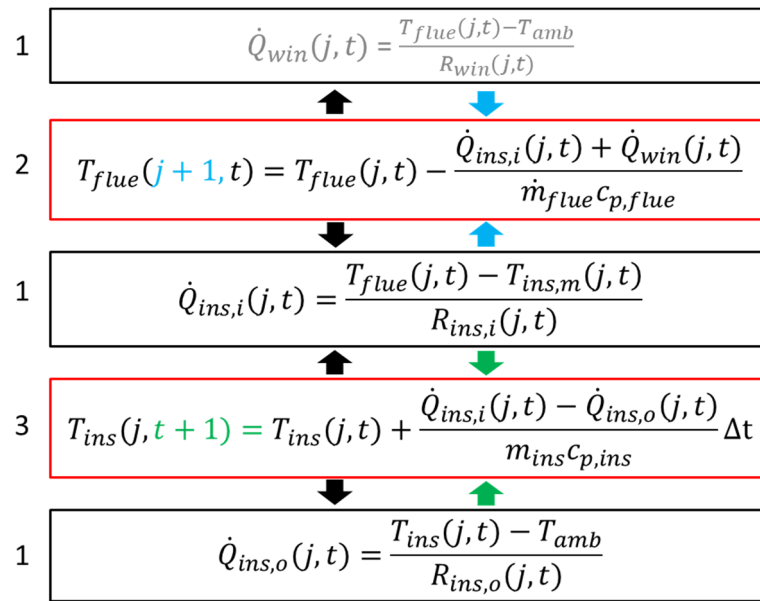


Figure 8. Calculation routine for the flue gas temperature at the combustion chamber outlet.

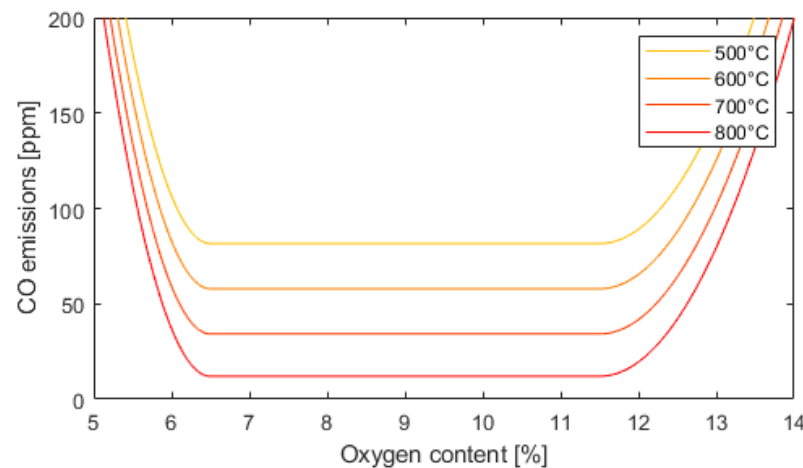


Figure 9. Average CO emissions as a function of the residual oxygen content for different temperatures in the combustion chamber.

CO emissions increase significantly when the critical oxygen content is no longer maintained (the “CO-edge” is reached). This behavior was also observed on the test stand of the pellet stove. The measured data were fitted to obtain a function of the CO emissions as a function of the combustion chamber temperature and the oxygen content.

2.5. Control Module

The exhaust gas temperature at the exit of the combustion chamber, the O₂ content and the CO content determined in the heat release module are used as the input for the controller. The controller determines the fan speed, the secondary air flap position and the pellet supply speed.

LabVIEW 2019 software was used on the test stand of the real stove for data acquisition and implementation of the control strategy. To avoid writing the control software code twice, it was decided to program the control strategy directly in LabVIEW and to integrate the code into the MATLAB–Simulink tool via a TCP/IP connection. The connection allows for the use of the same LabVIEW controller in the real measurement setup and in the model without modification.

3. Test Stove

To validate the results of the simulation tool, a test setup of a pellet stove with a primary energy consumption rate, or input, based on the fuel flow rate and heating value, of 1.8 up to 4 kW was realized. The stove development and design have been performed by our development partners BIOS BIOENERGIEYSTEME GmbH and RIKA Innovative Ofentechnik GmbH. In addition, the mass flows in the exhaust gas and in the primary and secondary air supply were measured. The mass flows of the combustion air, the exhaust gas mass flow and the fuel mass flow are recorded on the test rig. The temperature is measured at the combustion chamber outlet as well as at the inner and outer wall of the lateral fireclay bricks of the combustion chamber. To determine the combustion quality, the flue gas is analyzed via a standard measuring section (according to EN 14785). For comparison and validation of the simulation tool with the real stove, mainly the temperatures of the combustion chamber insulation, those of the hot flue gas at the combustion chamber outlet and the data of the flue gas analysis were used.

4. Results

The 0-D simulation tool allows for the simulation of a measurement lasting several hours in a few minutes (with normal computational power). In the following, simulations of different pellet feed frequencies and secondary air flap positions have been carried out to find an optimal operational point. Afterwards, a control strategy based on previous simulations has been created. The resulting controller has been tested by means of a representative load cycle which simulates the daily stove performance in real life [18] and been compared to the simulation results with constant secondary air flap position. Finally, to show the accuracy of the model, the controller was implemented on a real test rig and the results from the load cycle test were compared with the simulation.

4.1. Parameter Study

The simulation tool allows for the determination of the influence of different parameters such as primary and secondary air supply or pellet feed. As a first example, a critical minimum pellet feed frequency, which leads to increased CO-emissions can be identified. Additionally, the focus of the model is demonstrated: the identification of an optimized control algorithm using the secondary air flow as a control parameter.

4.1.1. Pellet Supply

A continuous pellet supply is important to keep CO emissions low. At an input of 4 kW, the effects on the CO emissions (blue) and the temperature at the outlet of the combustion chamber (red) were studied. When the number of pellets per insertion is increased, the pellet insertion frequency is decreased to keep an average input power of 4 kW. Simulated temperatures and CO emissions for a pellet feed every 1.2 s, 10 s, 20 s, and 30 s on average, after 6000 s of operation are shown in Figure 10. The simulation includes a statistical pellet feed function, described in the next section. A pellet insertion every 20 s on average (5 g per insertion) has comparable temperature fluctuations and CO emissions to a pellet insertion every 1.2 s on average (0.3 g per insertion). For a pellet insertion every 30 s on average (7.5 g) an increase in temperature fluctuations and increase in CO emissions, as compared to lower insertion frequencies, can be observed. A different number of pellets per insertion at an equal input power and hence lower frequency does not have a significant influence on temperature fluctuations and CO emissions unless the amount is equal to or lower than 5 g per insertion.

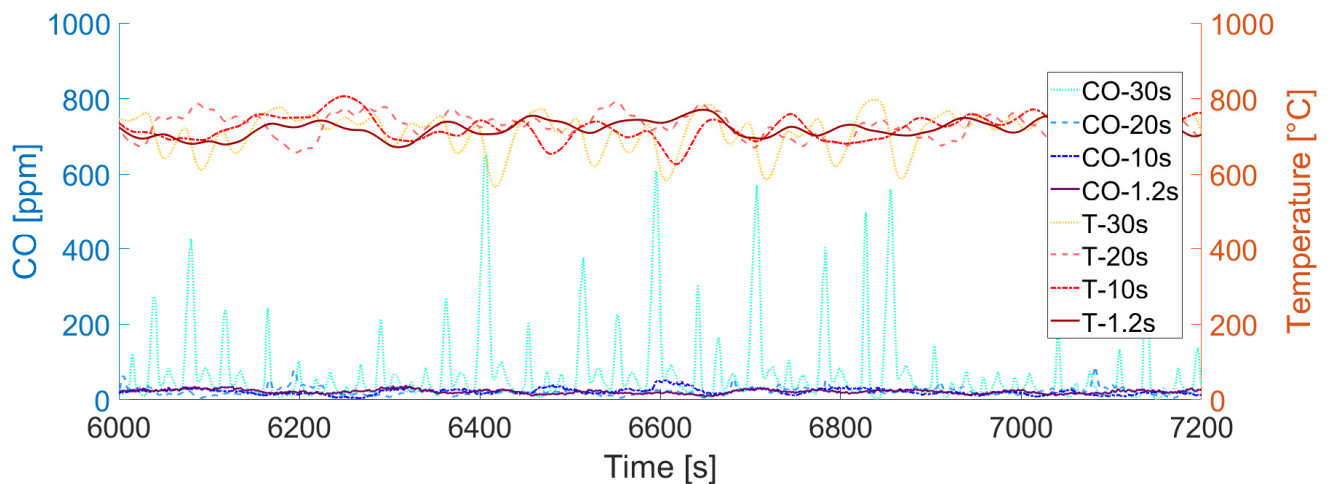


Figure 10. Combustion chamber temperature (T) and CO emissions (CO) after 6000 s of operation (4 kW input power) including a statistical pellet feed function. Pellet feed every 1 s, 10 s, 20 s and 30 s on average.

4.1.2. Effect of Secondary Air with Statistical Fuel Delivery

A statistical pellet supply function has been implemented in the model to simulate actual variations in the pellet mass supply, using a random number generator. The average mass flow of pellets corresponded to 4 kW thermal power. Figure 11 shows the elapsed time until a new pellet insertion occurs and its corresponding probability.

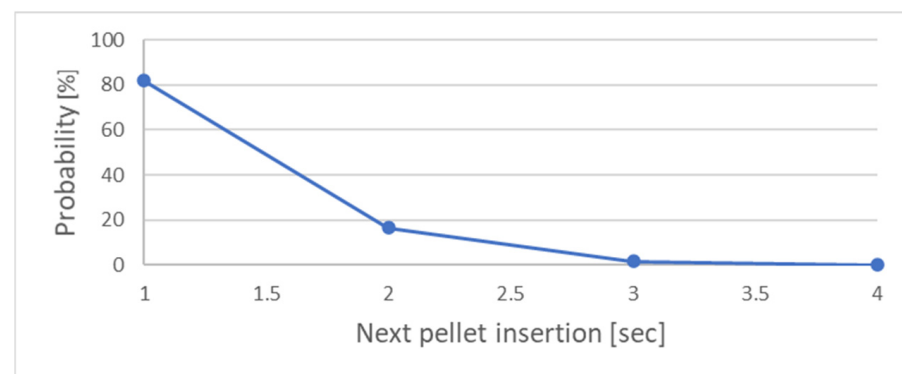


Figure 11. Probability of the pellet insertion depending on elapsed time since the last insertion.

A secondary air flap position leading to a good air/fuel ratio is essential to achieve combustion with low CO emissions. Figure 12 shows the simulated CO concentrations and temperatures at the combustion chamber outlet depending on different secondary air mass flows generated by varying the opening of the secondary air flap. The dashed lines show the standard deviation from the mean value (solid line) for the last hour during a 3 h simulation.

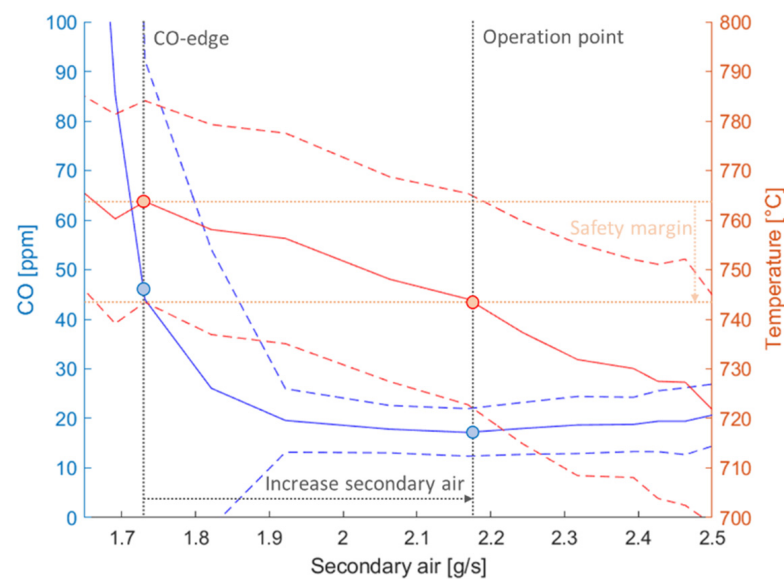


Figure 12. Influence of the secondary air supply to the temperature at the combustion chamber outlet (red) and CO emissions (blue) at 4 kW input power. Solid line represents the mean value and the dashed line the spectrum (standard deviation).

4.2. Development of a Control Strategy

With the help of the simulation tool, a control strategy was developed to achieve a maximum efficiency while keeping CO emissions low. The control strategy should be able to deal with load changes and other interferences such as a partial blockage of air holes leading to a reduction of the air supply or minor changes to the pellet feed frequency.

The controller is dependent on a CO sensor and a temperature sensor at the combustion chamber outlet. Value pairs of temperature and CO emissions for the last half hour of operation are acquired and used to create a function for the dependence of CO on temperature. This function needs to be updated constantly to react to interferences or changing operation conditions during the startup phase. With increasing temperature, a significant CO increase (CO-edge) can be identified as indicated in Figure 12 on the left side of the graph. The corresponding temperature minus a safety margin—necessary to deal with statistical fluctuations—determines the optimal operation point. To reach the optimal temperature, i.e., the maximum temperature with CO below a critical value, the secondary air must be increased. The CO-temperature curve is constantly adjusted with simulated or measured values from the last half hour. When running half an hour around the optimal operation point, the CO-edge is no longer visible in the CO-temperature curve. The algorithm searches for a new CO-edge by decreasing the primary air supply slowly.

The optimal temperature is adjusted by the controller by changing the position of the secondary air flap. If the temperature is too low, the flap closes, the amount of secondary air is reduced, the residual oxygen content in the exhaust gas drops and the exhaust gas temperature at the combustion chamber outlet rises. When the flap is opened, the system reacts in the opposite way. The system reaction to changes of the flap position is not immediate but depends on various delay factors. In order to improve the control stability, a PDI controller [19] was used. Equation (16) (on the left) shows an integral part of a conventional PID controller $Y_{I,PID}$ with deviation $e(\tau)$ to the temperature setpoint, integral factor K_I and the running time t . The PDI $Y_{I,PDI}$ controller (Equation (16), on the right) has incorporated damping elements which reduce oscillation compared to a conventional PID controller. The integral part of a PDI controller, $Y_{I,PDI}$ reduces the overshoot after a fast temperature increase, because the derivative of the temperature $dT(t)/dt$ multiplied by a factor K_D is subtracted.

$$Y_{I,PID} = \int_0^t K_I e(\tau) d\tau \rightarrow Y_{I,PDI} = \int_0^t K_I e(\tau) - K_D \frac{dT(t)}{dt} d\tau \quad (16)$$

4.3. Comparison between Constant Flap Position and Controlled Operation

A standardized load cycle [18] was simulated twice, once with a fully opened secondary air flap and once under controlled operation with a variable secondary air flap. The load cycle test was developed by a European consortium as part of a previous project with the aim of being able to map real user behavior in a standardized load cycle. The test cycle consists of sequences with a maximum input power ((a1) and (b)), with minimum input power (a2) and with medium input power (c). In between, there are two sequences in which the stove is not operated ((S1) and (S2)). The resulting exhaust gas temperatures in the load cycle at the outlet of the combustion chamber are shown in Figure 13. For better visibility of the temperature differences, moving averages have been calculated. The temperature for the sequences (a1), (b) and (c) could be increased.

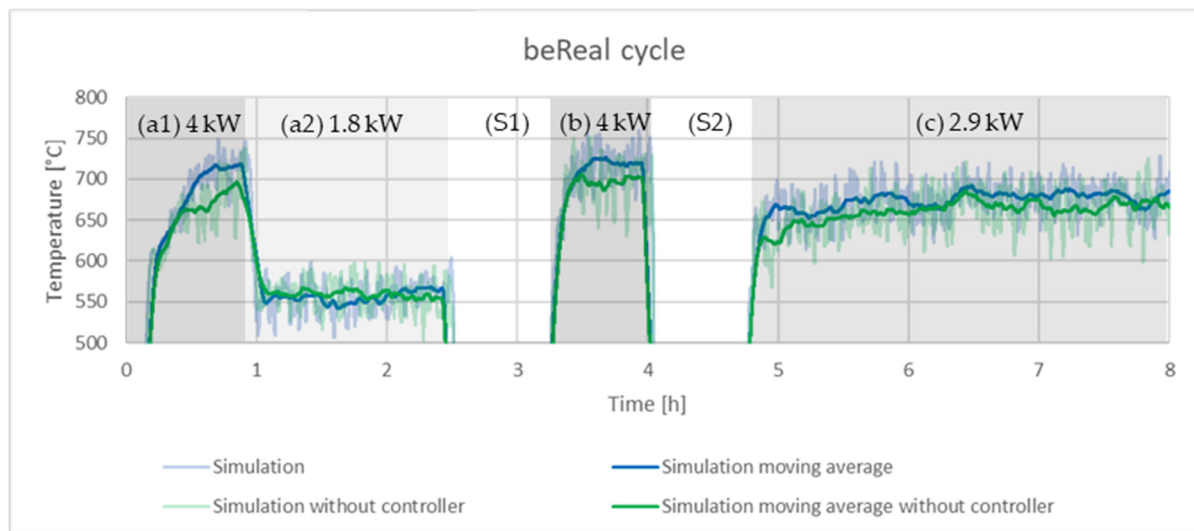


Figure 13. Load cycle simulations—comparison between an operation with fully open air flap (blue) and controlled operation (green).

A goal of the control algorithm is to keep CO emissions low while increasing the efficiency. The average oxygen content over the entire measurement period was reduced by 1.68% (Table 1) and the temperature was increased by 11.1 °C. Therefore, there was less excess air in the exhaust and the efficiency was increased, while the CO emissions remain at a comparable level. The standard deviation of the temperature and CO emissions indicate comparable fluctuations, while the fluctuations of oxygen are increased by 0.63%. A reason for this could be the changes of the secondary air flap position when the algorithm searches for a new optimal operation point in the control algorithm.

Table 1. Average oxygen and CO concentrations as well as temperatures at the outlet of the main combustion chamber and its corresponding standard deviations. The average and standard deviation were calculated over the sequences (a1), (a2), (b) and (c). The sequences (S1) and (S2) are not considered.

	Load	Without Control (STD)	With Control (STD)	Δ (STD)
O ₂	%	11.15 (1.65)	9.47 (2.28)	−15.1 % (+38.2%)
CO	ppm	120.5 (456.6)	134.4 (449.0)	+11.5 % (−1.5%)
T	°C	618.3 (108.6)	629.4 (112.0)	+11.1 °C (+3.4 °C)

4.4. Comparison between Measurements and Simulation

The controller was tested in the real stove and the results compared with the simulation. In a first step the temperatures and their frequencies are analyzed before the overall emissions and other measurement parameters are presented.

The temperature measured at the exit of the stove is influenced by flame radiation. This leads to a deviation between the measured temperature of the flue gas and the actual flue gas temperature. The calculated flue gas temperature in the model is not influenced by radiation. To adjust the calculated flue gas temperature to a measured value, a temperature-dependent correction factor for the heat loss across the combustion chamber was used.

The temperature curve for the simulation is shown in Figure 14 and closely follows the measurement.

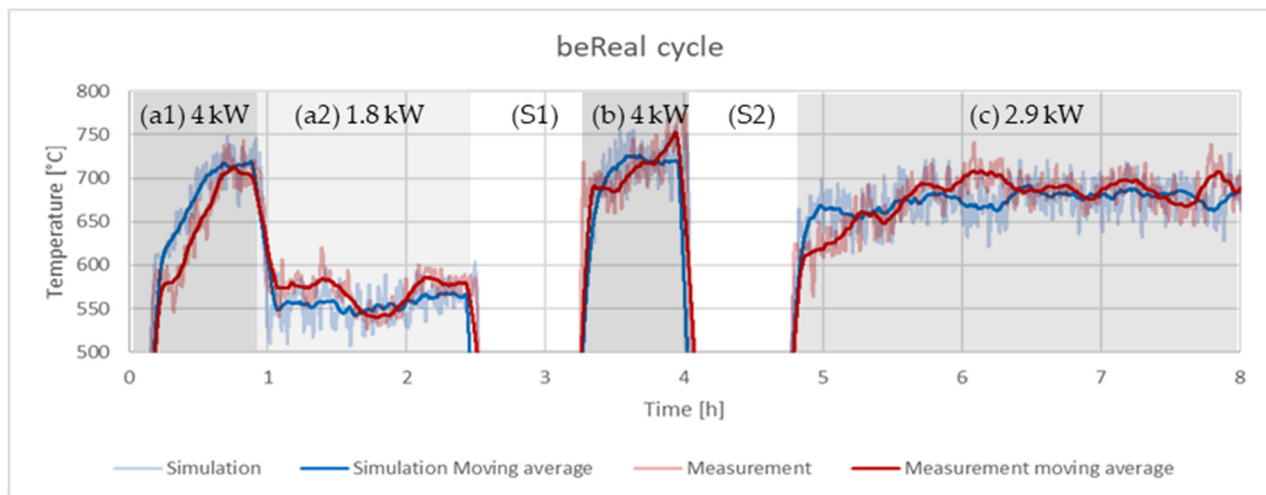


Figure 14. Comparison of the temperature development in the main combustion chamber according to a load cycle test performed (red) and a simulation (blue).

Averaged temperatures and their standard deviations around the moving average for different parts of the load cycle are shown in Table 2. The overall average is calculated without the off periods (S1) and (S2) in the load cycle. The temperature as a control parameter is very well represented with an average deviation of 2.1 °C. The fluctuations also show a small deviation of 0.2 °C over the entire measurement period. At the start during warmup, the average deviations from the model of 24.9 °C are highest and fluctuations around the mean value. Otherwise, the temperatures with the corresponding fluctuations (standard deviations) agree very well with a less-than-15 °C difference and a maximal difference in the standard deviation of 5 °C.

Table 2. Averaged temperatures at the combustion chamber outlet for different loads.

	Load	Simulation (STD)	Meas. (STD)	Δ (STD)
Overall Average	2.9 kW	629.4 (19.5)	631.5 (19.7)	+2.1 °C (+1.0%)
Warmup	(a1) 4 kW	586.8 (22.3)	561.9 (23.0)	−24.9 °C (+3.1%)
Part Load	(a2) 1.8 kW	560.9 (15.3)	574.1 (8.6)	+13.2 °C (−43.8%)
Full Load	(b) 4 kW	666.4 (33.9)	673.3 (36.1)	+6.9 °C (+6.5)
Part Load	(c) 2.9 kW	663.9 (14.1)	667.1 (14.2)	+3.2 °C (+0.7%)

From Table 2, conclusions may be made regarding the absolute temperatures and the amplitudes of the temperature fluctuations. Equally important for the development of a controller, however, is the correct reproduction of the frequencies which are shown for the combustion chamber temperature in Figure 15.

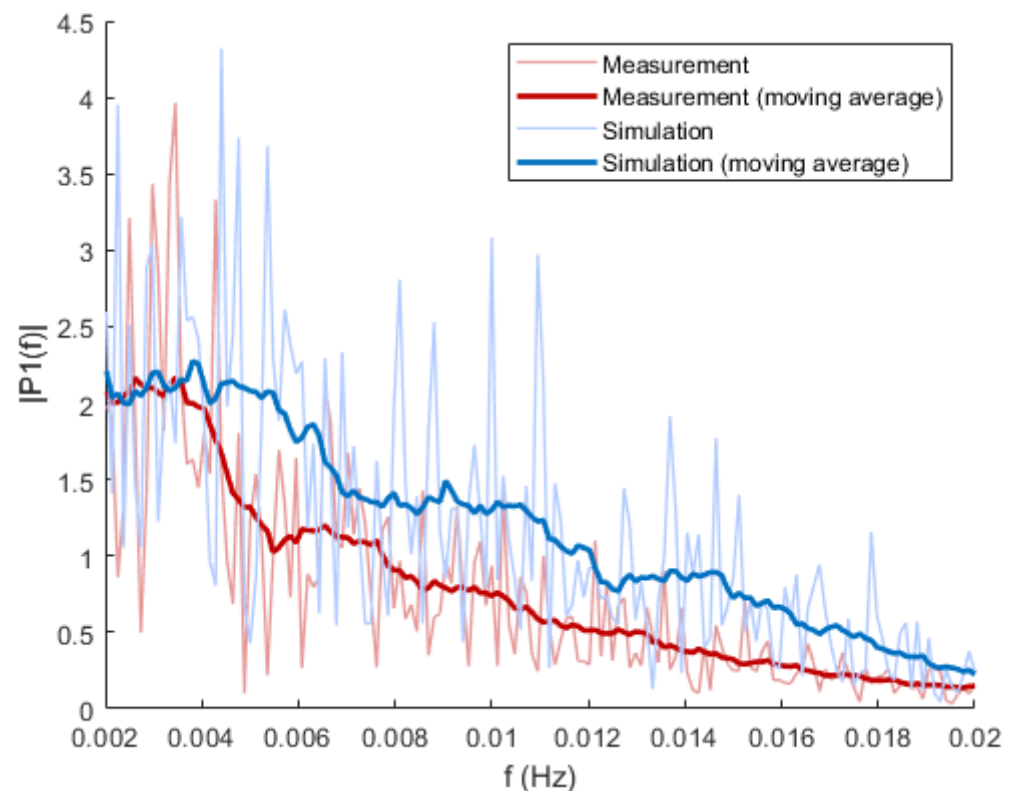


Figure 15. FFT analysis of combustion chamber temperature at 2.9 kW input power.

The temperature signals in the combustion chamber are sampled at a frequency of 1 Hz. A spectrum is then created using fast Fourier transformation (FFT), which covers the frequencies from 0.002 to 0.02 Hz.

Figure 15 shows the frequency spectra and the associated moving averages over 0.002 Hz. The sliding mean values (thick lines) show that the simulation and the measurement in the stove have comparable frequencies. However, the simulation does weigh frequencies above 0.004 Hz (250 s) more. The higher weighting means a larger amplitude for those frequencies and therefore higher fluctuations. If a control concept can deal with the increased fluctuations in the model, it can deal with real condition as well and is more robust.

All other parameters measured during the load cycle have been averaged over the whole cycle. The results of the measurement and simulation data are summarized in Table 3.

Table 3. Averaged values of the comparison between load cycle test and simulation results including the standard deviation (std).

	Unit	Simulation (STD)	Meas. (STD)	Δ (STD)
Secondary air flap	%	58.4 (13.8)	53.4 (17.4)	−5 % (+3.6%)
Primary air	g/s	0.34 (0.08)	0.31 (0.11)	−8.8 % (+37.5%)
Secondary air	g/s	1.54 (0.47)	1.18 (0.34)	−23.4 % (−27.7%)
Exhaust	g/s	2.05 (0.58)	2.08 (0.53)	+1.5 % (−8.6%)
O ₂	%	9.47 (2.28)	8.7 (2.37)	−8.1 % (+3.9%)
CO	ppm	134.4 (449.0)	159.1 (403.8)	+18.4 % (−10.1%)
Temperature combustion chamber	°C	629.4 (112.0)	631.5 (112.5)	+2.1 °C (+0.5 °C)

The primary air supply and the exhaust air are well reproduced on average with a deviation of 0.03 g/s. However, the secondary air has a larger difference. The reason is that the stove has a significant amount of false air, which is not measured. In the model there is

no false air and thus, larger amounts of secondary air are necessary. The average oxygen content in the exhaust gas is simulated to be 0.77% higher compared to the measurement. The CO emissions, depending on the residual oxygen and temperature, are simulated as already shown in Figure 9. The CO edge (sudden increase in CO emissions caused by lack of oxygen) for the simulation is at a higher residual oxygen content in the exhaust gas compared to the measurement in the stove, leading to a different operational point (higher amount of residual oxygen). Important for designing a control strategy are the oscillations of the exhaust gas composition (O_2 and CO), which can be described with the standard deviations. These deviations show a good agreement between measurement and simulation.

5. Discussion

Developing a completely new control algorithm usually requires significant testing on a prototype pellet stove, which is time-consuming and costly. In order to shorten the required laboratory test time, a simulation tool of the combustion process in a pellet stove was developed. The process of wood combustion in a pellet stove is extremely complex and involves several reactions that take place simultaneously. With the new simulation tool programmed in MATLAB–Simulink, the process has been simplified so that the simulation can be run on a normal office laptop and still achieve realistic behavior of the simulated stove at transient and steady-state operation. The control algorithm was programmed in LabView; through specific interfaces the same code could be used to run the simulation and to control the prototype stove. This allowed a quick optimization with the simulation tool and a confirmation test on the real oven. This was possible despite the relatively simple architecture of the simulation tool and its simple description of the combustion process. By using the new simulation tool, we propose a much faster development cycle for new control algorithms for pellet stoves.

A simple model makes it possible to represent the combustion process sufficiently well to test different control algorithms. Linking the LabVIEW controller with the MATLAB–Simulink model via a TCP/IP connection was crucial to test the same controller in the model and on a real test rig. Additionally, the model can be used to quantify effects of variations in other process parameters, for example the impact of fluctuations in the pellet feed.

The fit formula used for the burning behavior of a pellet gave a good agreement with measured pellet mass loss. The fit formula could be used for the simulation of a drying process in a more complex simulation tool considering the water concentration gradient within a piece of wood during the drying process.

The temperature in the combustion chamber and the CO emissions of a standardized load cycle test [18] can be well reproduced by the model. The average temperature fluctuations over the whole cycle (standard deviation to the moving average) are comparable with a simulated fluctuation of 19.5 °C compared to the measured 19.7 °C. The CO emissions are simulated to have a standard deviation of 334% around the mean value over the whole cycle, while the measurements have a smaller standard deviation of 254% around the mean value.

The model is not able to simulate operational phases with large time intervals between individual pellet supply correctly, and thus, such phases were not included in the comparison between the model and test results. The reason for the model's inability to describe such phases is that only the superposition of the combustion of single pellets is being simulated. In the real stove a glowing pellet bed in the first combustion zone can be established during operation, which can maintain heat release after a stoppage in pellet supply. The single pellet combustion in the model leads to a fast temperature decrease after a pellet supply stoppage in the model. In the stove however, the pellet bed is still hot, and hence the cooling is slower. At an operation temperature above 500 °C, the behavior of the stove, including load changes, can be accurately simulated, if the pellet supply is not interrupted. For the investigated loads of this study (1.8 kW to 4 kW) the temperature

is always above 500 °C, and therefore a simulation of the glow bed was not necessary to develop and test control strategies.

The established model can be used to develop control strategies for other two staged, wood combustion systems. The model simulates the transient behavior of a pellet stove and system dependency on important process control parameters (actuators) such as the air flows, CO emissions and temperatures. The implemented dependencies are generally valid and can be used to develop a control strategy for any pellet stove. To adjust the model to given pellet stove, specific transport parameters need to be known or estimated (e.g., the heat transfer and heat storage properties of the insulation material as well as an estimate of radiative heat losses). For the air distribution module, measurements of the primary and secondary air supply as well as the pressure inside the combustion chamber are needed. Finally, a probability function describing the pellet supply must be found. In the heat release module, a function describing an O₂/O curve for different temperatures needs to be found within a measurement campaign.

Author Contributions: T.G. and T.S. designed and developed the study. D.L. and J.S. performed the experiments. F.M., D.L. and J.S. programmed the simulation tool. Portions of the work were carried out during the master studies of J.S. All authors have read and agreed to the published version of the manuscript.

Funding: This research was funded by the Swiss Federal Office of Energy (BFE) (SI/501839-01) as part of the ERA-NET project “Development of a new low-cost low-emission micro-scale pellet stove with advanced process control” (Acronym: LowEmi-MicroStove) with Reference Number: BEN12-18-14, which was coordinated by I. Obernberger.

Data Availability Statement: Data are available from the corresponding author.

Acknowledgments: This work was carried out within the scope of the ERA-NET Bioenergy programme “12th ERA-NET Bioenergy Joint Call/2nd additional BESTF3 Joint Call on Biomass as an important pillar within energy systems and the circular economy”. We thank our project partners BIOS BIOENERGIESYSTEME GmbH, Rika Innovative Ofentechnik GmbH and Lamtec Mess- und Regeltechnik für Feuerungen GmbH for their valuable contributions. We would like to thank our colleagues Dieter Winkler and Josef Wüest for their help during the measurement campaign and their valuable input regarding the setup and development of the simulation tool.

Conflicts of Interest: The authors declare no conflict of interest.

References

1. Sturc, M. Renewable energy. Analysis of the latest data on energy from renewable sources. *Eurostat Stat. Focus* **2012**, *2012*, 44–2012.
2. Schwabl, M.; Schwarz, M.; Figl, F.; Carvalho, L.; Staudinger, M.; Kalb, W.; Schmidl, C.; Haslinger, W. Development of a biomass heating device for low energy and passive houses. *Manag. Env. Qual.* **2013**, *24*, 652–666. [\[CrossRef\]](#)
3. Georges, L.; Skreiberg, Ø.; Novakovic, V. On the proper integration of wood stoves in passive houses: Investigation using detailed dynamic simulations. *Energy Build.* **2013**, *59*, 203–213. [\[CrossRef\]](#)
4. Georges, L.; Skreiberg, Ø.; Novakovic, V. On the proper integration of wood stoves in passive houses under cold climates. *Energy Build.* **2014**, *72*, 87–95. [\[CrossRef\]](#)
5. Mandl, C.; Obernberger, I.; Koessl, M.; Lustenberger, D.; Strebel, T.; Winkler, D. Clean and Efficient Low Emission Micro-Scale Pellet Stove with Advanced Control. In Proceedings of the 30th European Biomass Conference & Exhibition, Online, 9 May 2022.
6. Mandl, C.; Obernberger, I.; Volz, F.; GmbH, W. *Guidelines for Automated Control Systems for Stoves*; Technical University of Denmark: Lyngby, Denmark, 2017; p. 29.
7. Göllies, M. *Grundlagen für die modellbasierte Regelung einer Biomasse-Feuerung*; Südwestdeutscher Verlag für Hochschulschriften: Saarbrücken, Germany, 2009.
8. Bauer, R.; Göllies, M.; Brunner, T.; Dourdoumas, N.; Obernberger, I. Modellierung der Druck- und Volumenstromverhältnisse in einer Biomasse-Feuerung (Modelling of Pressures and Volume Flows for a Biomass Furnace). *Automatisierungstechnik* **2007**, *55*, 404–410. [\[CrossRef\]](#)
9. Mehrabian, R.; Scharler, R.; Obernberger, I. Effects of pyrolysis conditions on the heating rate in biomass particles and applicability of TGA kinetic parameters in particle thermal conversion modelling. *Fuel* **2012**, *93*, 567–575. [\[CrossRef\]](#)
10. Koraïem, M.; Assanis, D. Wood stove combustion modeling and simulation: Technical review and recommendations. *Int. Commun. Heat Mass Transf.* **2021**, *127*, 105423. [\[CrossRef\]](#)
11. Gianfelice, G.; Canu, P. On the mechanism of single pellet smouldering combustion. *Fuel* **2021**, *301*, 121044. [\[CrossRef\]](#)

12. Biswas, A.K.; Rudolfsson, M.; Broström, M.; Umeki, K. Effect of pelletizing conditions on combustion behaviour of single wood pellet. *Appl. Energy* **2014**, *119*, 79–84. [[CrossRef](#)]
13. Hartwig Künzel, M. Bauphysikalische Problemstellung. Ph.D. Thesis, Universität Stuttgart, Stuttgart, Germany, 1994; p. 68.
14. Grosse, L. *Arbeitsmappe für Mineralölingnieure*; VDI Verlag: Düsseldorf, Germany, 1962.
15. Sénéchal, U. *Holzverbrennung in Kaminöfen mit Keramikfilter-experimentelle Untersuchungen und Mathematische Modellierung*; Technische Universität Dresden: Dresden, Germany, 2013.
16. Kaltschmitt, M.; Hartmann, H.; Hofbauer, H. *Energie aus Biomasse*; Springer: Wien, Austria, 2016.
17. Deutsch, M.; Göller, M.; Zemmann, C.; Zlabinger, S. *Modellbasierte Regelung von Scheitholzkesseln mit Pufferspeicher*; Österreichische Forschungsförderungsgesellschaft mbH: Vienna, Austria, 2018.
18. Reichert, G.; Schmidl, C. *Final Report: Definition of Suitable Measurement Method and Advanced Type Testing Procedure for Real Life Conditions*; BF2020+: Graz, Austria, 2016.
19. Wüest, J. Selbstadaptiver PID-Regler. EP 0 974 880 A1 26 January 2000.